Benchmarking LHC background particle simulation with the CMS triple-GEM detector

M. Abbas,[n] M. Abbrescia,[t] H. Abdalla,[h,j] A. Abdelalim,[h,k] S. AbuZeid,[h,i] A. Agapitos,[d]
A. Ahmad,[af] A. Ahmed,[q] W. Ahmed,[af] C. Aimè,[y] C. Aruta,[t] I. Asghar,[af] P. Aspell,[ak]
C. Avila,[f] I. Azhgirey,[ag] J. Babbar,[p] Y. Ban,[d] R. Band,[am] S. Bansal,[p] L. Benussi,[v]
V. Bhatnagar,[p] M. Bianco,[ak] S. Bianco,[v] K. Black,[ap] L. Borgonovi,[u] O. Bouhali,[al]
D. Bozzato,[ak,1] A. Braghieri,[y] S. Braibant,[u] S. Butalla,[aq] S. Calzaferri,[y] M. Caponero,[v]
F. Cassese,[x] A. Castaneda,[ae,*] N. Cavallo,[x] S.S. Chauhan,[p,*] A. Colaleo,[t]
A. Conde Garcia,[ak] M. Dalchenko,[al] A. De Iorio,[x] G. De Lentdecker,[a] D. Dell Olio,[t]
G. De Robertis,[t] W. Dharmaratna,[aj] S. Dildick,[al,2] B. Dorney,[a] R. Erbacher,[am] F. Fabozzi,[x]
F. Fallavollita,[ak] A. Ferraro,[y] D. Fiorina,[y] E. Fontanesi,[u] M. Franco,[t] C. Galloni,[ap]
D. Gancarcik,[ak,3] P. Giacomelli,[u] S. Gigli,[y] J. Gilmore,[al] M. Gola,[q] M. Gruchala,[ak]
A. Gutierrez,[an] R. Hadjiiska,[c] T. Hakkarainen,[l] J. Hauser,[ao] K. Hoepfner,[m] M. Hohlmann,[aq]
H. Hoorani,[af] T. Huang,[al] P. Iaydjiev,[c] A. Irshad,[a] A. Iorio,[x] F. Ivone,[m] W. Jang,[ab]
J. Jaramillo,[g] V. Jha,[s] A. Juodagalvis,[ad] E. Juska,[al] B. Kailasapathy,[ah,ai] T. Kamon,[al]
Y. Kang,[ab] P. Karchin,[an] A. Kaur,[p] H. Kaur,[p] H. Keller,[m] H. Kim,[al] J. Kim,[aa] S. Kim,[ab]
B. Ko,[ab] A. Kumar,[q] S. Kumar,[p] H. Kumawat,[s] I. Kurochkin,[ag] N. Lacalamita,[t] J.S.H. Lee,[ab]
A. Levin,[d] Q. Li,[d] F. Licciulli,[t] L. Lista,[x] K. Liyanage,[aj] F. Loddo,[t] M. Luhach,[p] M. Maggi,[t]
Y. Maghrbi,[ac] N. Majumdar,[r] K. Malagalage,[ah] S. Malhotra,[al] S. Mallows,[n] S. Martiradonna,[t]
N. Mccoll,[ao] C. McLean,[am] J. Merlin,[t] M. Misheva,[c] D. Mishra,[s] G. Mocellin,[m] L. Moureaux,[a]
A. Muhammad,[af] S. Muhammad,[af] S. Mukhopadhyay,[r] M. Naimuddin,[q] P. Netrakanti,[s]
S. Nuzzo,[t] R. Oliveira,[ak] L. Pant,[s] P. Paolucci,[x] I.C. Park,[ab] L. Passamonti,[v] G. Passeggio,[x]
A. Peck,[ao] A. Pellecchia,[t] N. Perera,[aj] L. Petre,[a] H. Petrow,[l] D. Piccolo,[v] D. Pierluigi,[v]
G. Raffone,[v] M. Rahmani,[aq] F. Ramirez,[g] A. Ranieri,[t] G. Rashevski,[c] B. Regnery,[am]
M. Ressegotti,[y,4] A. Riabchikova,[ag] C. Riccardi,[y] M. Rodozov,[c] E. Romano,[y] C. Roskas,[b]
B. Rossi,[x] P. Rout,[r] D. Roy,[aq] J.D. Ruiz,[g] A. Russo,[v] A. Safonov,[al] A.K. Sahota,[p]
D. Saltzberg,[ao] G. Saviano,[v] A. Shah,[q] A. Sharma,[ak] R. Sharma,[q] T. Sheokand,[p]
M. Shopova,[c] F.M. Simone,[t] J. Singh,[p] U. Sonnadara,[ah] E. Starling,[a] B. Stone,[ao] J. Sturdy,[an]
G. Sultanov,[c] Z. Szillasi,[o] D. Teague,[ap] D. Teyssier,[o] T. Tuuva,[l] M. Tytgat,[b] I. Vai,[w]

---

[1]Also at Karlsruhe Institute of Technology, Karlsruhe, Germany.
[2]Now at Rice University, Houston, Texas, U.S.A.
[3]Also at Czech Technical University (CZ), Prague, Czech Republic.
[4]Now at INFN Sezione di Genova, Genova, Italy.

N. Vanegas,[g] **R. Venditti,**[t] **P. Verwilligen,**[t] **W. Vetens,**[ap] **A.K. Virdi,**[p] **P. Vitulo,**[y] **A. Wajid,**[af]
D. Wang,[d] **K. Wang,**[d] **I.J. Watson,**[ab] **N. Wickramage,**[aj] **D.D.C. Wickramarathna,**[ah] **S. Yang,**[ab]
Y. Yang,[a] **U. Yang,**[aa] **J. Yongho,**[z] **I. Yoon,**[aa] **Z. You,**[e] **I. Yu**[z] **and S. Zaleski**[m]

[a] *Université Libre de Bruxelles, Bruxelles, Belgium*

[b] *Ghent University, Ghent, Belgium*

[c] *Institute for Nuclear Research and Nuclear Energy, Bulgarian Academy of Sciences, Sofia, Bulgaria*

[d] *Peking University, Beijing, China*

[e] *Sun Yat-Sen University, Guangzhou, China*

[f] *University de Los Andes, Bogota, Colombia*

[g] *Universidad de Antioquia, Medellin, Colombia*

[h] *Academy of Scientific Research and Technology — ENHEP, Cairo, Egypt*

[i] *Ain Shams University, Cairo, Egypt*

[j] *Cairo University, Cairo, Egypt*

[k] *Helwan University, also at Zewail City of Science and Technology, Cairo, Egypt*

[l] *Lappeenranta University of Technology, Lappeenranta, Finland*

[m] *RWTH Aachen University, III. Physikalisches Institut A, Aachen, Germany*

[n] *Karlsruhe Institute of Technology, Karlsruhe, Germany*

[o] *Institute for Nuclear Research ATOMKI, Debrecen, Hungary*

[p] *Panjab University, Chandigarh, India*

[q] *Delhi University, Delhi, India*

[r] *Saha Institute of Nuclear Physics, Kolkata, India*

[s] *Bhabha Atomic Research Centre, Mumbai, India*

[t] *Politecnico di Bari, Università di Bari and INFN Sezione di Bari, Bari, Italy*

[u] *Università di Bologna and INFN Sezione di Bologna, Bologna, Italy*

[v] *Laboratori Nazionali di Frascati INFN, Frascati, Italy*

[x] *Università di Napoli and INFN Sezione di Napoli, Napoli, Italy*

[y] *Università di Pavia and INFN Sezione di Pavia, Pavia, Italy*

[w] *Università di Bergamo and INFN Sezione di Pavia, Pavia, Italy*

[z] *Korea University, Seoul, Korea*

[aa] *Seoul National University, Seoul, Korea*

[ab] *University of Seoul, Seoul, Korea*

[ac] *College of Engineering and Technology, American University of the Middle East, Dasman, Kuwait*

[ad] *Vilnius University, Vilnius, Lithuania*

[ae] *Universidad de Sonora, Hermosillo, Mexico*

[af] *National Center for Physics, Islamabad, Pakistan*

[ag] *Institute for High Energy Physics of NRC Kurchatov Institute, Protvino, Russia*

[ah] *University of Colombo, Colombo, Sri Lanka*

[ai] *Trincomalee Campus, Eastern University, Sri Lanka, Nilaveli, Sri Lanka*

[aj] *University of Ruhuna, Matara, Sri Lanka*

[ak] *CERN, Geneva, Switzerland*

[al] *Texas A&M University, College Station, U.S.A.*

[am] *University of California, Davis, Davis, U.S.A.*

---

*Corresponding author.

[an]Wayne State University, Detroit, U.S.A.

[ao]University of California, Los Angeles, U.S.A.

[ap]University of Wisconsin, Madison, U.S.A.

[aq]Florida Institute of Technology, Melbourne, U.S.A.

E-mail: castaned@cern.ch, schauhan@cern.ch

ABSTRACT: In 2018, a system of large-size triple-GEM demonstrator chambers was installed in the CMS experiment at CERN's Large Hadron Collider (LHC). The demonstrator's design mimicks that of the final detector, installed for Run-3. A successful Monte Carlo (MC) simulation of the collision-induced background hit rate in this system in proton-proton collisions at 13 TeV is presented. The MC predictions are compared to CMS measurements recorded at an instantaneous luminosity of 1.5×10^{34} cm^{-2} s^{-1}. The simulation framework uses a combination of the FLUKA and GEANT4 packages. FLUKA simulates the radiation environment around the GE1/1 chambers. The particle flux by FLUKA covers energy spectra ranging from 10^{-11} to 10^4 MeV for neutrons, 10^{-3} to 10^4 MeV for γ's, 10^{-2} to 10^4 MeV for $e^{\pm}$, and 10^{-1} to 10^4 MeV for charged hadrons. GEANT4 provides an estimate of the detector response (sensitivity) based on an accurate description of the detector geometry, the material composition, and the interaction of particles with the detector layers. The detector hit rate, as obtained from the simulation using FLUKA and GEANT4, is estimated as a function of the perpendicular distance from the beam line and agrees with data within the assigned uncertainties in the range 13.7-14.5%. This simulation framework can be used to obtain a reliable estimate of the background rates expected at the High Luminosity LHC.

KEYWORDS: Detector modelling and simulations I (interaction of radiation with matter, interaction of photons with matter, interaction of hadrons with matter, etc); Interaction of radiation with matter; Micropattern gaseous detectors (MSGC, GEM, THGEM, RETHGEM, MHSP, MICROPIC, MICROMEGAS, InGrid, etc); Detector modelling and simulations II (electric fields, charge transport, multiplication and induction, pulse formation, electron emission, etc)

Contents

1 Introduction

Most of the modern high energy particle physics experiments use colliding particle beams or a single beam impinging on a fixed target. Due to the high collision rate and the interaction of beam particles with matter, a hostile radiation environment is created. This radiation field is mainly composed of low energy neutrons, photons (γ), electrons/positrons ($e^{\pm}$) and charged hadrons, namely kaons ($K^{\pm}$), pions ($\pi^{\pm}$), and protons (p) [1]. These particles are commonly referred to as background particles. Due to the large interaction cross sections, background particles can cause damage to detector elements and front-end electronics [2]. Additionally, they can induce spurious signals that degrade the detector performance. A strategy for mitigating radiation effects is crucial to the design and upgrade of the LHC experimental facilities [3]. The strategy described in this paper uses estimates obtained with Monte Carlo (MC) simulation and measurements. Dedicated data taking campaigns are used to collect background data to understand the detector behaviour with respect to variations in the experimental parameters such as the instantaneous luminosity and the location of the detector element with respect to the interaction point. Additionally, new detector technologies are studied using high radiation doses in dedicated facilities such as the CERN High Energy AcceleRator Mixed Field (CHARM) [4] and the Gamma Irradiation Facility (GIF++) [5] at CERN. A set of detectors based

on the triple-GEM technology [6] is being installed in Muon system of the Compact Muon Solenoid (CMS) detector [7] for Run-3 and the Phase-2 (High Luminosity LHC) muon upgrade program [8]. A similar technology has been adopted for the upgrade of the ALICE TPC [9]. Background studies are crucial to understand the impact of radiation on the detector performance. Detector simulations (GEANT4 [10] and FLUKA [11] in this study) that reproduce the measurements will allow us to evaluate the impact of radiation in muon detection performance. For instance, an overestimation of the neutron flux would lead to a larger probability of misreconstruction of muons. To study the radiation environment and its impact on the detector performance, dedicated simulation tools involving a description of complex physics processes and particle decay chains are used.

The present study for the CMS GE1/1 detector system extends our previous work [8, 12] and provides a foundation for future studies of the response to background particles by other detector systems in CMS and other experiments. This study includes a detailed simulation strategy and methodology, an accurate detector description, and the response of a triple-GEM detector as a function of the incident particle's kinematic properties. Variations of the detector configuration are considered to show the validity of the estimates and robustness of the simulation model. Furthermore, the simulation model is compared with experimental data collected in 2018 by the GE1/1 slice test at the CMS detector. Reliable modeling of the detector response will serve for future studies relevant to the preparation for the High Luminosity LHC [13] where the luminosity will increase by one order of magnitude and different detector technologies will be exposed to a harsher radiation environment. This work can be useful for simulation of the response of other muon systems to background particles [14, 15].

This article is organized as follows: section 2 gives an overview of the CMS GE1/1 GEM detector and the experimental setup of the detectors in the CMS experiment. Section 3 presents a simulation study of the response of a single triple-GEM detector to various particles and the simulation framework. The response and its variation as a function of energy and angle of incident particles are compared with previous simulation studies. In section 4, results for the response of superchambers for a given geometry and the actual readout conditions during the slice test are presented. A prediction of hit rates using the FLUKA simulation and its systematic uncertainties are given in sections 5 and 6. A comparison of these predictions with measurements taken during LHC running is presented in section 7, followed by a summary in section 8.

2 Overview of the CMS GE1/1 detector and slice test

2.1 CMS GE1/1 detector

The GE1/1 station in each muon endcap is upstream of the Muon Endcap Station-1 (ME1/1), as shown in figure 1 in the R-z plane. Here, R is the perpendicular distance from the beamline. The CMS coordinate system is a right-handed cartesian coordinate system with the origin at the collision point, the x-axis pointing towards the center of the LHC ring, the y-axis pointing upwards and the z-axis along the beam direction. The polar angle θ is measured from the positive z-axis to the x-y plane and the azimuthal angle ϕ is measured from the positive x-axis in the x-y plane. The pseudorapidity η is defined as $\eta = -\ln[\tan(\theta/2)]$ and gives the information about angle of particle relative to beam axis.

The GE1/1 detector system in each endcap consists of 36 superchambers where each superchamber is comprised of a pair of trapezoidal-shaped triple-GEM detectors, covering a ϕ slice of

10.15°. The superchambers are arranged in a staggered configuration with an overlap of 0.075° to provide full 2π coverage in ϕ. The superchamber design maximizes the detection of muons. The superchambers alternate in ϕ between a long version covering a pseudorapidity region of 1.55 < $|\eta|$ < 2.18 and a short version covering 1.61 < $|\eta|$ < 2.18 (figure 2 right). The use of long and short superchambers provides maximal η coverage within the mechanical envelope of the existing endcap. The dimensions of the long and short chambers are summarized in table 1. The triple-GEM detector of a superchamber closer to the interaction point of the pp collision is called Layer-1 and the other detector of the pair is called Layer-2, as shown in figure 2 right. Moreover, each triple-GEM detector is segmented into eight η partitions, referred to as i_η (=1 to 8) and each partition has 384 radial readout strips.
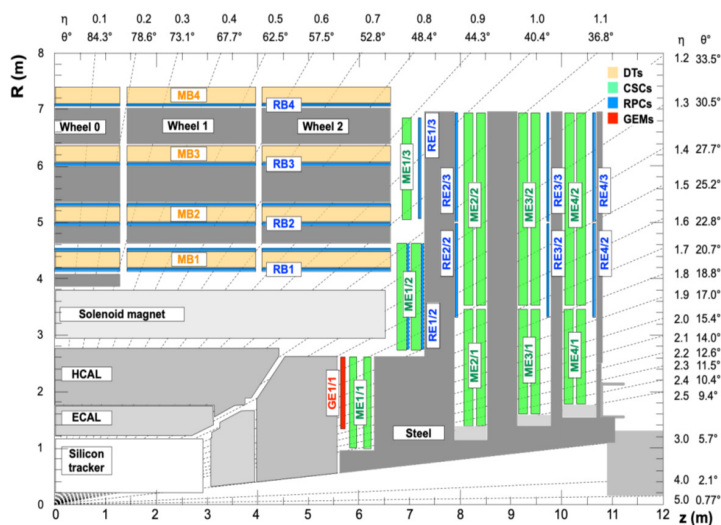

Figure 1. An *R*-*z* cross section of a quadrant of the upgraded CMS detector highlighting the location of the GE1/1 station (in red) with triple-GEM technology in the muon endcap region. Also shown are the previously existing muon stations, i.e., drift tubes (MB), cathode strip chambers (ME), and resistive plate chambers (RB, RE), and the flux-return steel yoke (dark areas).

Table 1. Dimensions of long and short trapezoidal-shaped triple-GEM detector.

Configuration	Long Chamber	Short Chamber
Height	1283.0 mm	1135.0 mm
Short Base Length	282.2 mm	282.2 mm
Long Base Length	510.0 mm	483.7 mm

2.2 GE1/1 slice test

Five triple-GEM pre-production superchambers were installed in the CMS experiment and exposed to pp collisions at 13 TeV in the period from 2017 to 2018 as shown in figure 3. This served as a demonstrator to obtain operational experience with the detector control system (DCS), the data
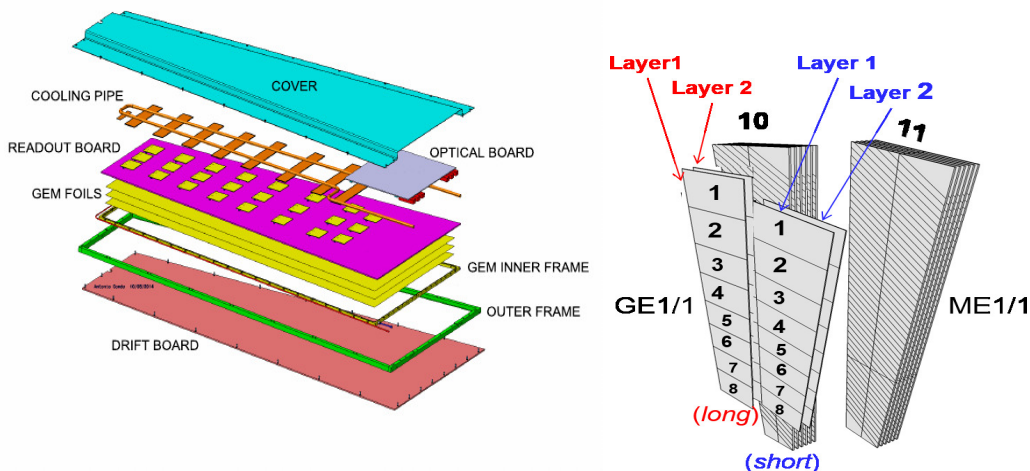
Figure 2. Single triple-GEM detector with various parts (left). Long (red) and short (blue) superchambers are mounted upstream of the ME1/1 station and cover the ranges in pseudorapidity $1.55 < |\eta| < 2.18$ and $1.61 < |\eta| < 2.18$, respectively, in a staggered configuration, with an overlap of $0.075°$(right).

acquisition (DAQ) system, and the data quality monitoring (DQM) system, as well obtaining the first data to assess the performance of the detector with pp collisions. The design of these demonstrator superchambers is very similar to that of the final superchambers installed in the CMS endcap except for the use of an improved version of the front-end electronics mounted on the chamber. The improved version was realized by increasing the values of the protection resistor of each VFAT channel and the decoupling resistor for the chamber HV filter [16]. Figure 2 left shows a schematic drawing of the demonstrator chamber.

Superchambers 27, 28, 29, 30 ($\Delta\phi = 40°$) in Slot-1 (shown in figure 3) were used to detect muons, while superchamber 1 ($\Delta\phi = 10°$) in Slot-2 tested the upgraded electronics and a new GEM high voltage (HV) system [17] to be used in Run-3. The GE1/1 slice test chambers were operated at a gas gain amplification of $\sim 1 \times 10^4$ with Ar/CO_2 gas mixture. Strip readout thresholds of 3 fC (i_η = 3-8), 4.0 fC (i_η = 2), and 8.8 fC (i_η = 1) were applied to the VFAT electronics based on electronic noise level. These thresholds are further discussed in detail in sections 3 and 4.

It should be noted that an irreversible channel loss was observed from April 2017 through December 2018 caused by discharges from one of the GEM foils nearest to the anode plane. As a result, only Layer-2 of superchamber 28 was operating with minimal channel loss ($< 0.5\%$) throughout the slice test. The channel loss occurred both in the presence and the absence of particle beams in the LHC. Further details of the slice test setup and performance studies based on the data can be found in [18].

3 Response of a single triple-GEM detector to collision-induced background particles

In this section, the sensitivities (defined below) of a single triple-GEM detector of the CMS GE1/1 design, without electronics and aluminium frame, are evaluated and compared with results reported
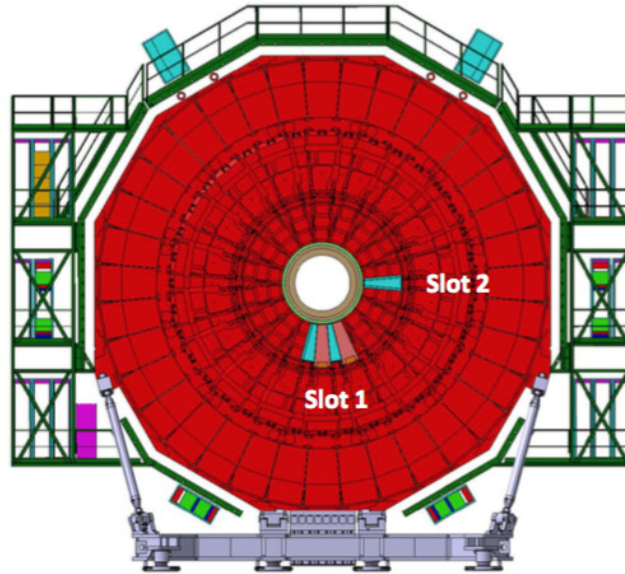
Figure 3. Schematic drawing of the negative muon endcap, showing the location of the five slice test superchambers.

in the GE1/1 Technical Design Report [8] and with studies done at the CHARM facility [12]. It should be noted that the response of the single triple-GEM detector is affected by material of other triple-GEM detectors within the superchamber.

3.1 Single triple-GEM detector geometry

The detector response is modeled using a GEANT4 [10] simulation with the geometry of a triple-GEM detector [8] and incident background particles with properties consistent with those generated in pp collisions at the LHC. A single triple-GEM detector is shown in figure 2. Chamber dimensions and material composition are presented in tables 1 and 2, respectively. Figure 4 shows a simplified schematic transverse view of a triple-GEM detector's gas gap configuration.
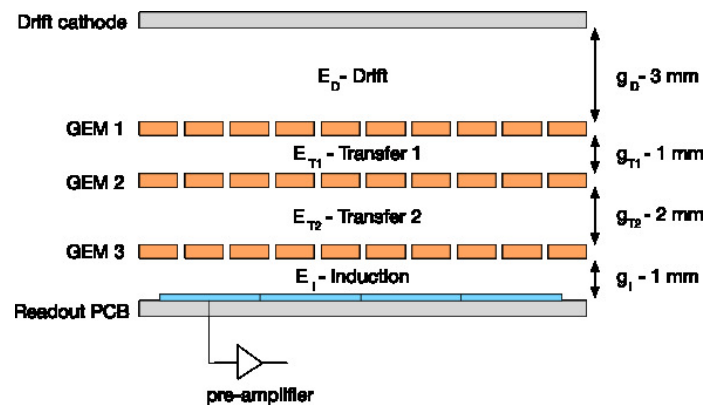

Figure 4. Representation of a transverse view of a triple-GEM detector.

Table 2. Material and dimensions of the different layers in a single triple-GEM detector.

Layer	z-Dimensions	Material
Drift Board	35 μm / 3.2 mm / 35 μm	Copper / FR4 / Copper
Drift Gap	3 mm	Ar / CO_2
GEM1	5 μm / 50 μm / 5 μm	Copper / Kapton / Copper
Transfer-1 Gap	1 mm	Ar / CO_2
GEM2	5 μm / 50 μm / 5 μm	Copper / Kapton / Copper
Transfer-2 Gap	2 mm	Ar / CO_2
GEM3	5 μm / 50 μm / 5 μm	Copper / Kapton / Copper
Induction Gap	1 mm	Ar / CO_2
Readout Board	35 μm / 3.2 mm / 35 μm	Copper / FR4 / Copper

3.2   Simulation

The physics processes and decay chains are simulated using GEANT4 version 10.6 with the physics list recommended for standard HEP processes (FTFP_BERT_HP). The list includes all standard electromagnetic processes, the Bertini-style cascade for hadrons (<5 GeV), and the FTF (Fritiof) model for high energies (>4 GeV). It also includes a dedicated model for neutrons below 20 MeV [19].

The simulation setup has "source planes" that generate primary particles. The source planes are the same size as the drift board of the GEM detector and are located at a distance of 3 mm from the detector, on both sides. This configuration captures all possible incident angles and path lengths of the primary particles hitting the surface of the detector and traversing its sensitive volume. The response of the detector to the primary incident particles is estimated separately on each side for each source plane. The average is used to estimate the final response of the detector. Although the simulation considers the interaction of particles and the creation of secondaries in the different gaps of the triple-GEM detector, the detector response is extracted from the first two gas gaps, namely the drift and transfer-1 gaps (figure 4).

The signal induction is due to the production of a charged particle inside the detector originating from the interaction of neutral or charged background particles (e.g., neutrons, γ's, electrons, and charged hadrons). Other meaningful processes in signal evolution (such as electron drift, multiplication, charge transfer, and electronic response) are not covered in this study. Studies of the optimization of signal detection [20] using other simulation packages were used for the detailed design of the CMS GEM detectors.

The detector response is characterized using the *sensitivity* variable. *Sensitivity* is defined as the probability for a charged particle to deposit energy in the sensitive volume (e.g., Ar/CO_2 gas mixture), and to produce primary ionized electrons [8, 12]. Primary electrons go through a multiplication process, so that the charge is large enough to be detected by a readout system with charge thresholds. The charge threshold is related to the energy deposit required to separate signal

from noise. Hence the sensitivity can be expressed as:

$$Sensitivity = \frac{N_{\text{hits}}}{N_{\text{total}}} \tag{3.1}$$

Here, N_{total} is the total number of incident particles entering the active surface of a GEM detector from any direction and N_{hits} is the number of total "hits" recorded above a certain energy threshold. The "hits" are counted for a given incident particle at a given incident energy and angle through the triple-GEM detector.

The simulated energy depositions in the first two gaps of a triple-GEM detector are converted to charge depositions using corresponding amplification factor, and required to be above the minimum threshold value of the VFAT chip. Although the readout electronics have a threshold of 3 fC, a value of 1.69 fC is used, corresponding to one electron in the drift gap, in order to study the effects of low levels of noise. Later in section 4.2, the energy thresholds are set to match the operational configuration of the GE1/1 chambers in CMS.

The minimum energy deposits required are estimated as follows:

- The gas gain amplification (G) was set to 1×10^4, corresponding to 24, 22, and 20 multiplications, respectively, in the transfer-1, transfer-2, and induction gaps.

- The readout thresholds for the strips were set to 1.69 fC for $i_\eta = 1$ to 8. Hence, to achieve this threshold a total of ~ 10547 (= 1.69 fC $/1.6021\times 10^{-19}$ C) electrons are required.

- The minimum average number of electrons required to be produced in the drift gap and the transfer-1 gap are 1 (= $10547/G$) and 24 (= $10547/G^{2/3}$), respectively.

- The effective average energy required to remove an electron due to ionization for an Ar/CO_2 gas mixture (in the ratio of 70/30) is $\langle W_i \rangle = 28.1$ eV [21, 22]. Thus, energy losses of 28.1 eV and 674.4 eV (= 24$\times$ 28.1 eV) are needed to count as "hits" in drift and transfer-1 gaps, respectively. Those electrons produced in the drift and transfer-1 gaps are amplified by 10^4 and 440, respectively, at the readout strips. If the energy loss of a particle, simulated by GEANT4, is above the threshold, a "hit" is counted for (N_{hits}) in equation (3.1).

Due to the fact that GEANT4 does not report charged particles with a track length less than 0.7 mm [23], instead of counting secondary charged particles, we impose requirements on the amount of energy deposited in the gaps. This procedure is consistent with previously published results in ref. [12].

The detector response depends on the particle type, its kinematic properties, and the composition of the material in which the particle interacts. The dominant energy loss processes for neutrons are inelastic scattering at high energy (> 10 MeV), elastic scattering at intermediate energy (10^{-5} to 10 MeV), and neutron capture at low energy (< 10^{-5} MeV). The dominant processes for γ's are pair production at high energy (> 10 MeV), Compton scattering at intermediate energy (10^{-1} - 10 MeV), and the photoelectric effect at low energy (< 10^{-1} MeV). The dominant processes for $e^\pm$ are bremsstrahlung at high energy (> 1 MeV) and ionisation at low energy (< 1 MeV). Neutral particles (neutrons and γ's) interact before they produce a charged particle. The estimated sensitivity, as a function of kinetic energy and angle, is presented as a 2D map for neutrons (figure 5

left) and γ's (figure 5 right). The one-dimensional projection of sensitivity as a function of incident energy for different particles at normal incidence to the detector is presented in figure 6 left. The sensitivity as a function of the incident angle for different particle types, at two energy values (1 and 100 MeV), is presented in figure 6 right.
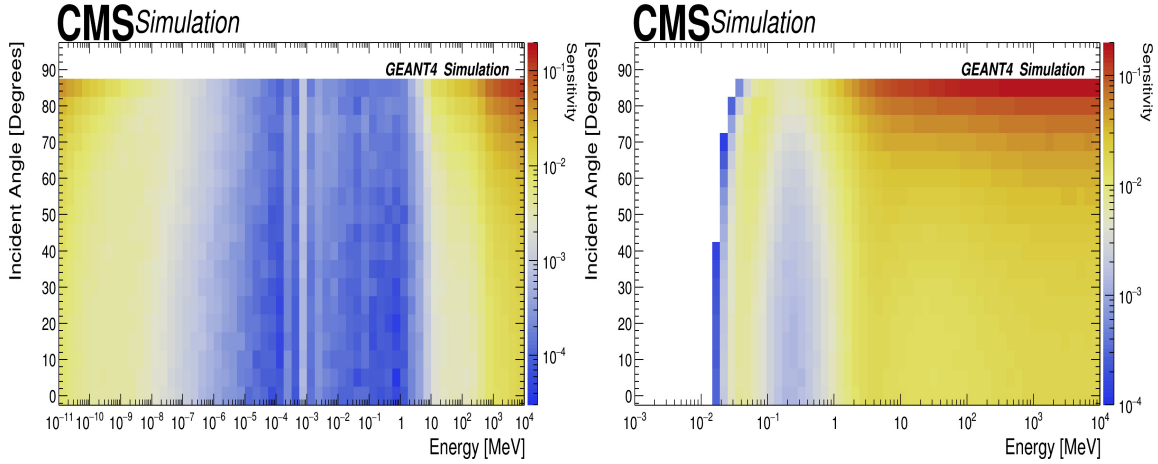

Figure 5. Sensitivity map for neutrons (left) and photons (right). The *x*-axis is kinetic energy and the y-axis is incident angle.
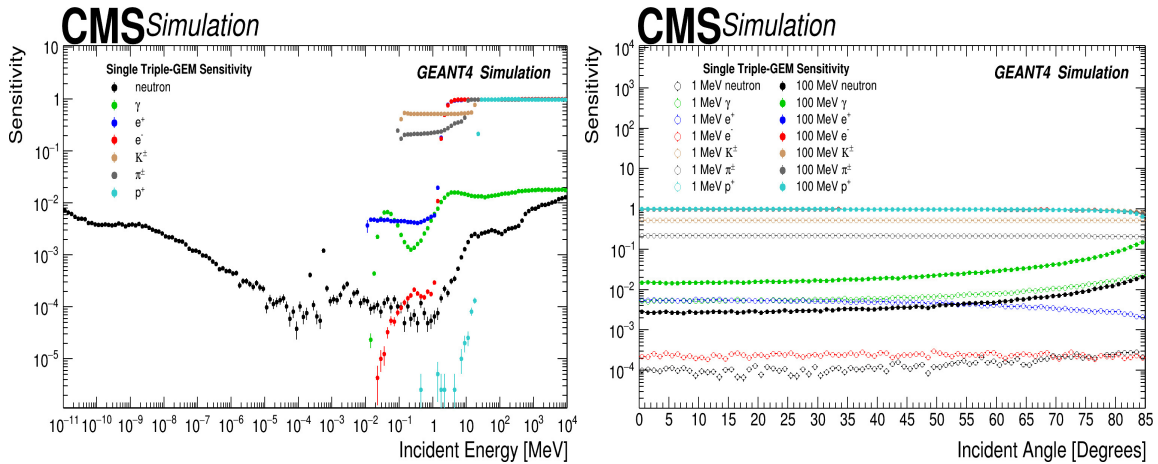

Figure 6. Sensitivity as a function of kinetic energy, for neutrons, photons and electrons, at normal incidence to the detector (left). Sensitivity as a function of incident angle for different types of particles for energy values of 1 MeV and 100 MeV (right).

The sensitivity is strongly dependent on the energy and incidence angle. The probability for an interaction is correlated to the detector width and the incidence angle. If the incidence angle increases the particle will traverse a larger distance inside the detector, so more material will be available as target for the interaction. The probability to interact is also process and energy dependent. To estimate the sensitivity, we take into account the energy spectrum of the incident particles, the energy dependent interaction probability, and the path length.

Sensitivities are obtained using large simulated samples with $O(10^7)$ events. The statistical uncertainty depends on the type of particle under study and the region in the sensitivity map. Statistical uncertainties lie in the ranges 0-16% for neutrons, 0-2.1% for γ's, and 0-10.0% for $e^\pm$.

It is important to note that the sensitivities were obtained without constraints from a particular radiation environment. The only information considered was the energy ranges for the different types of particles. Thus, the results can be used for any facility in which similar triple-GEM detectors are installed [12].

The sensitivities for a single triple-GEM detector, shown in figure 6 left, are independent of the shape of the surface of the detector. These results are qualitatively similar and quantitatively compatible with those presented in ref. [12]. The main difference, for neutron sensitivity at low energies, is attributable to several reasons. The GEANT4 version used in this simulation has updated modeling for thermal neutrons. Energy thresholds for drift and transfer-1 gaps were applied in this study but not in the previous one. Lastly, the previous study simulated a detector with an additional layer of Kapton (50 µm) and FR4 (1.2 mm).

The sensitivity for photons found here is consistent with that found in the previous study. Note that a GEM detector that is part of a superchamber installed in the CMS experiment will have a response different from that of the single chamber considered here. In the following sections, the background modeling is adapted to the characteristic radiation environment of the CMS experiment and the specific detector geometry of the GE1/1 muon upgrade project.

4 Collision-induced background particles on the GE1/1 chambers

The prediction of background rate in the GE1/1 detectors requires two components: the simulation of the radiation environment and the detector response. The radiation environment is simulated with FLUKA for collision of the LHC proton beams with a center of mass energy of 13 TeV in the configuration of the CMS experiment. The simulation models particle interactions and transport through the different layers of the CMS detector. The estimation of detector response follows an approach that is similar to that described in section 3, but using the geometry of a superchamber. Both components are described in the following sections.

4.1 Radiation environment for GE1/1

The information for incoming particles reaching the GE1/1 system is extracted from a FLUKA simulation for the conditions during data-taking in Run-2, with instantaneous luminosity of 1.5×10^{34} cm^{-2} s^{-1}. The cross section of the CMS detector geometry used in the FLUKA simulation is shown in figure 7 top-left. A key property estimated with the FLUKA simulation is the flux of particles: the number of particles per unit area and per unit time weighted for their tracklength in a volume defined by the detector of interest. This distribution is presented in figure 7 top-right. Other important distributions that characterize the incoming particles are those for energy, shown in figure 7 bottom-left, and incident angle, shown in figure 7 bottom-right. These distributions are needed for the subsequent GEANT4 simulation.

The results in figure 7 are consistent with an earlier study using the FLUKA simulation [24]. The major contribution in the region where the GE1/1 detectors are located comes from low energy neutrons (10^{-11} to 10^4 MeV), γ's (10^{-3} to 10^4 MeV), $e^\pm$ (10^{-2} to 10^4 MeV) and charged hadrons
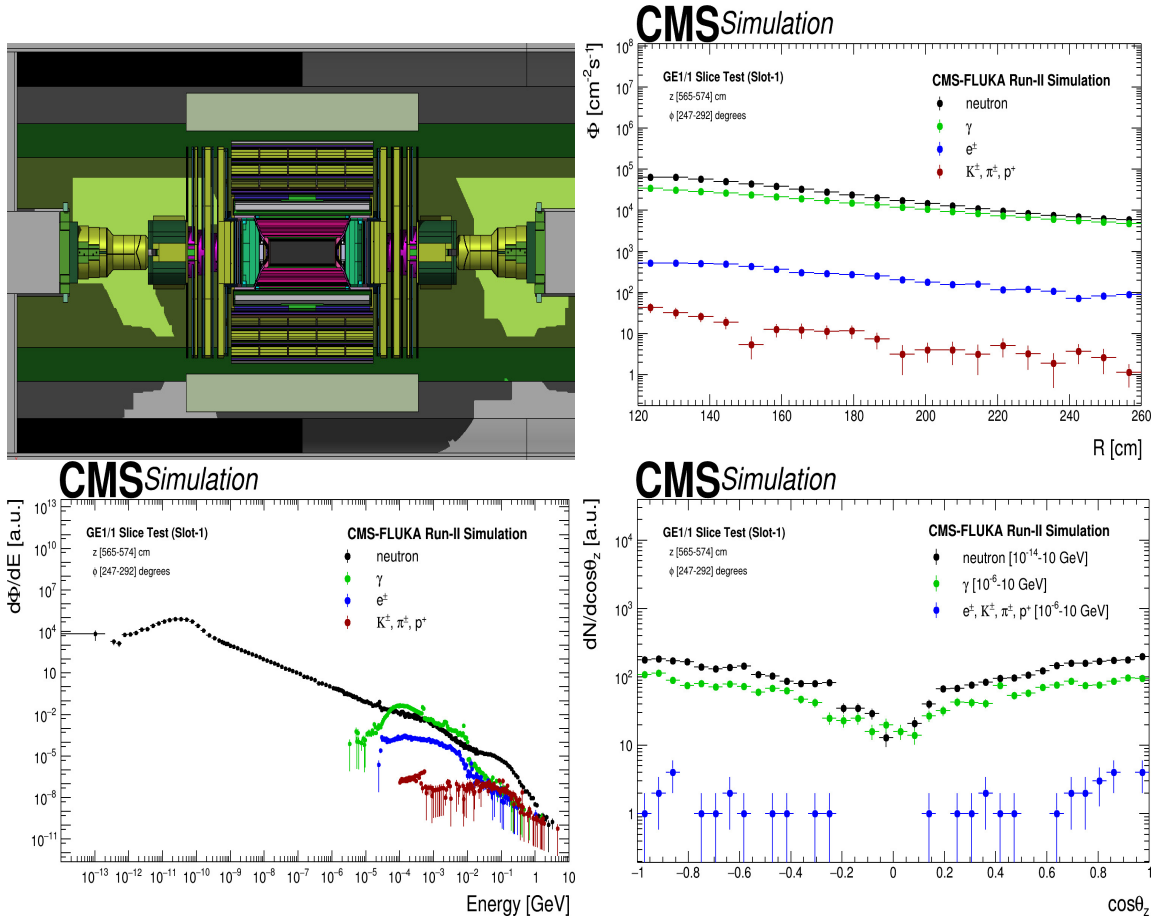
Figure 7. CMS geometry used in FLUKA simulation run v3.31.4.2 (top-left). Flux of particles, normalized to the instantaneous luminosity, arriving at the GE1/1 volume (top-right). Energy spectra of incoming particles (bottom-left) and distribution of direction cosine with respect to the normal to the detector surface for different particles (bottom-right).

(10^{-1} to 10^4 MeV). Minor contributions to the radiation field, such as muons from gauge boson decays, are neglected as their production cross sections are an order of magnitude lower than those shown in figure 7.

4.2 Detector response for a superchamber

The detector response to background radiation depends on all the materials of the triple-GEM detector, including the electronics, cooling system, and mechanical support. The triple-GEM detectors used in the CMS experiment have additional components compared to the simple triple-GEM configuration described in section 3. Table 3 lists some of these important additional components and their details. For this study, a long chamber configuration is used, as shown in tables 1 and 2. The superchamber has a total thickness of 73.1 mm, including a space of 3.7 mm between the two detectors.

Each triple-GEM detector unit has a GEM Electronics Board (GEB) with the readout electronics and a cooling system that consists of cooling pads and cooling pipes. The cooling pipes contain

circulating chilled water. Copper is used for the cooling pipes and pads because of its good thermal conductivity. A main component of the readout electronics for a superchamber are the VFAT-3 ASICs, based on the earlier Very Forward ATLAS and TOTEM (VFAT) ASICs [25, 26] and an Opto-Hybrid board. The VFAT-3s are used for reading, digitizing and processing the signals from the 384 strips of each η-sector of a superchamber layer. The Opto-Hybrid board is plugged into the GEB and contains Giga-Bit Transceiver (GBT) chip sets, optical receivers and transmitters, and a Field Programmable Gate Array (FPGA). Further details of the front-end electronics can be found in [8]. Figure 8 shows a GEANT4 based image of a superchamber, as used in this study.

Table 3. Additional material, layers and their dimensions used in the triple-GEM detector configuration in the CMS experiment.

Layer	z-Dimensions	Material
GEB	0.1 mm / 0.9 mm	Copper / FR4
VFAT and Opto-Hybrid	1.0 mm / 1.6 mm	FR4 / FR4
Cooling Pads	1.0 mm	Copper
Cooling Pipes	8.0 mm external, 6.0 mm internal	Copper (Filled with H_2O)
Spacers	3.0 mm / 1.0 mm / 2.0 mm / 1.0 mm	FR4
External Frame	7.2 mm	FR4
Aluminium Frame	11.5 mm	Aluminium
Cover	1.0 mm	Aluminium

The sensitivity is calculated by simulating the detailed detector configuration as described above, that is the same configuration used in the GE1/1 slice test [18]. Thresholds used in simulation are summarized in table 4 and estimated as discussed in section 3.2 but with an energy deposit threshold corresponding to 3 fC, as used in the slice test [18].

Table 4. The energy thresholds and related parameters used in the simulation of the drift and the transfer-1 gaps of the triple-GEM detector configuration. The effective gain is set to 1×10^4 and the charge threshold for readout is 3 fC.

Parameters	Drift Gap	Transfer-1 Gap
Minimum no. of electrons in the gap	2	43
Energy thresholds	56.2 eV	1.21 keV

5 Collision-induced background hit rates in GE1/1 superchambers

The hit rate is defined as the number of particles detected per unit of time in single chamber. In the slice test, the hit rate was measured for the GE1/1 superchambers as a function of instantaneous luminosity and detector area [18]. The hit rate is one of the most important quantities to measure for detector calibration and monitoring. It depends on the convolution of particle flux and sensitivities
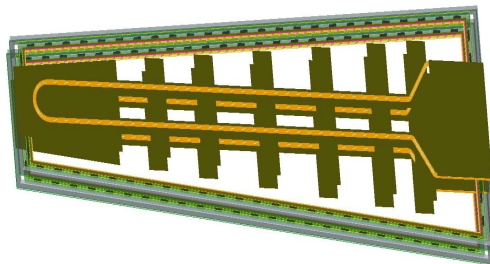
Figure 8. GEANT4 visualization of a superchamber containing two triple-GEM detectors.

for each particle type (neutrons, γ's, e$^{\pm}$, charged hadrons) as functions of energy and incident angle, as described in equation (5.1).

$$\text{Hit Rate} = \sum_{type} \text{Sensitivity}(type, E, \theta) \otimes \text{Flux}(type, E, \theta, R) \tag{5.1}$$

Here *type* is the kind of particle (*i.e.* neutrons, γ's, $e^{\pm}$ and charged hadrons), E is the energy of the incident particle and θ is the angle with respect to the normal to the detector surface. The perpendicular distance from the beamline is denoted by R. The particle flux is estimated using FLUKA as presented in figure 7 top-right and multiplied by an average sensitivity. The average sensitivity is obtained from the convolution of the sensitivity at a given energy and incident angle with the normalized abundance of particles at that energy and incident angle. The convolution over a given energy range gives the average sensitivity. The FLUKA simulation provides the information needed for all possible particle types arriving from different directions at a given position and time. The average sensitivity is used to convert the particle flux into total hits at that position.

The simulation technique used here for the sensitivity estimation is similar to that described in section 3. The main difference is that here we have a superchamber and additional material due to the presence of an extra triple-GEM detector. This affects the sensitivity of the other detector layers since sensitivity is measured for incident particles arriving at the superchamber surface from different directions. The sensitivities for Layer-2 of the superchamber, as a function of the energy of the primary incident particles arriving at the chamber surface, is shown in 9 for neutrons, photons, electrons/positrons and charged hadrons. It is convoluted over all possible incident angles and contribution from incident primary particles reaching the chamber surface from both sides are used.

The average sensitivity, estimated using the energy spectrum of the incident background particles, and the sensitivity for different energies are presented in table 5 for both Layer-1 and Layer-2. The method of using the average sensitivity is preferred over obtaining the sensitivity for different η-sectors because the detectors have a uniform response for each η-sector, as verified with X-rays during quality control tests [27].

The effect of detector material and configuration on the sensitivity can be seen by comparison of figure 6 left for the simplified geometry and figure 9 for the superchambers in the CMS experiment.

6 Systematic uncertainties

The accuracy of the sensitivity estimates relies on the correct description of the physics processes and on realistic detector modeling. The physics processes considered in this simulation are well
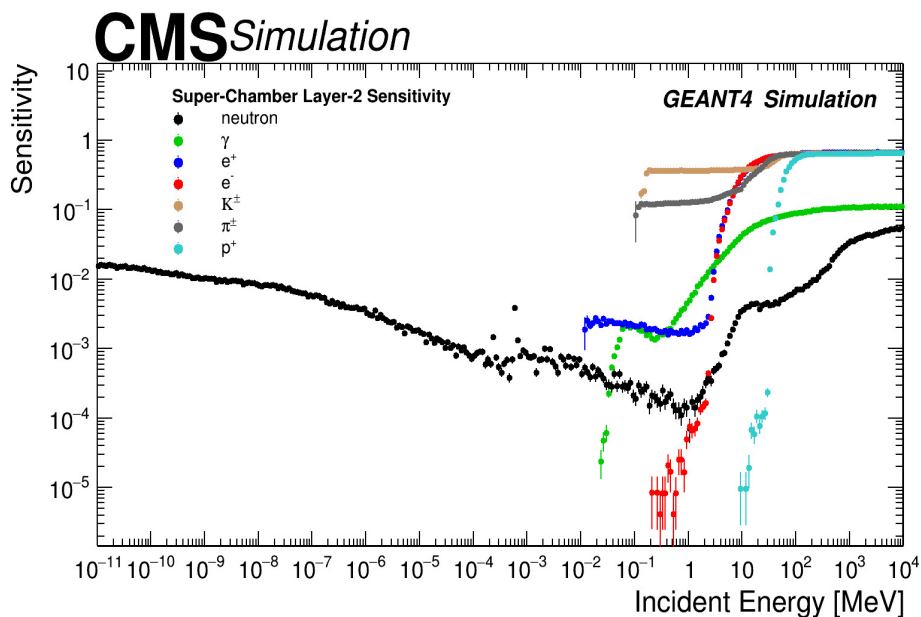
Figure 9. Sensitivity of Layer-2 as a function of incident energy for different particles. The sensitivity is convoluted over all possible incident angles.

Table 5. Average Sensitivity for each type of particle for Layer-1 and Layer-2 of the superchamber configuration used for data taking in 2018.

Particle	Average Sensitivity of Layer-1 (%)	Average Sensitivity of Layer-2 (%)
Neutron	0.64 ± 0.01 (stat.)	0.76 ± 0.01 (stat.)
γ	0.28 ± 0.01 (stat.)	0.22 ± 0.01 (stat.)
$e^{\pm}$	1.24 ± 0.04 (stat.)	0.31 ± 0.01 (stat.)
Charged Hadrons ($K^{\pm}, \pi^{\pm}, p$)	26.29 ± 1.24 (stat.)	24.29 ± 1.14 (stat.)

known and have been validated in the GEANT4 framework in several studies reporting comparisons with experimental data [28, 29]. To quantify the impact of the detector modeling on the sensitivity estimates the following parameters are varied.

- Drift Gap Width (DGW) variations could arise from mechanical deformations during detector assembly. Variations [8] of $\pm 10\%$ are used in the simulation for both layers of the superchamber. The impact on the average sensitivity of Layer-2 is shown in table 6.

- Gas Mixture Proportion (GMP) for the Ar/CO_2 (in the ratio 70/30) gas was monitored during detector operation and quality control testing and found to be negligible. However, conservative variations of (60/40) and (80/20) were considered in the simulation. The impact on the estimated average sensitivity of Layer-2 is shown in table 6.

The impact of the parameter variations depends on the type of incident particle, kinetic energy and incident angle. We found that a single detector is less sensitive compared to the experimental configuration. The impact of parameter variations on the sensitivity for different energy ranges is also estimated. The energy ranges for neutrons are low energy (LE) from 10^{-11} to 10^{-2} MeV, intermediate energy (IE) from 10^{-2} to 1 MeV, and high energy (HE) from 1 to 10^4 MeV. The energy ranges for γ's, $e^{\pm}$, and charged hadrons are LE from 10^{-2} to 1 MeV and HE from 1 to 10^4 MeV. For neutrons, the maximum variation in sensitivity due to GMP variations is 1.0% for LE, 5.6% for IE, and 4.6% for HE. For γ's, $e^{\pm}$, and charged hadrons the variation in LE (HE) is estimated to be 0.8% (0.5%), 2.1% (0.3%), and 1.2% (0.1%), respectively. For DGW uncertainties, variations are similar to those for GMP, except for the neutron case in the IE region for which the statistics are low.

The systematic uncertainty is also evaluated arising from changes in the setup of the primary source near the surface of the detector. The distance of the source surface from the detector is varied by ± 2 mm from the nominal value of 3 mm and the average sensitivity is re-calculated to measure the impact on the hit rate. A total variation of 0.5-0.8%, 0.0-1.0%, 0.2-0.4%, and 3.9-8.8% on the average sensitivity is estimated for neutrons, γs, $e^{\pm}$, and charged hadrons, respectively. These uncertainties are also summarized in table 6.

Table 6. Variations of simulation parameters and their impact on estimated average sensitivity. The change in sensitivity is relative to that obtained using the average sensitivity of Layer-2 shown in table 5.

Parameters	Values for Variations	Impact on average sensitivity of Layer-2 (in %)			
		Neutron	γ	$e^{\pm}$	Charged Hadrons
DGW	Drift Gap: 2.7 mm	0.6	1.4	1.0	0.5
	Drift Gap: 3.3 mm	0.3	0.4	0.0	0.6
GMP	Ar/CO_2 (60/40)	1.0	0.4	0.3	0.5
	Ar/CO_2 (80/20)	0.1	0.9	0.9	0.2
source z-position	1 mm	0.6	0.4	0.9	4.0
from superchamber	5 mm	1.0	1.4	0.9	9.9

Another systematic uncertainty comes from variation of the x-y dimensions of the source planes. The maximum variation for a 10% larger size of the source planes is about 1.3% or less for any type of incident particle. A 10% smaller size gives a maximum variation of 6.7% or less.

The uncertainties described in table 6 for different types of incident particles result in uncertainties on the hit rate. The overall uncertainty on the hit rate is dominated by neutron and photon contributions.

The systematic uncertainty associated with the particle flux is estimated by comparing the Run-2 scenario in FLUKA with an alternative scenario. In this alternative scenario, the material composition of the shielding in front of the Hadron Forward (HF) calorimeter is changed, replacing borated polyethylene by non-borated polyethylene; this change impacts the number of particles reaching the muon stations. The uncertainty is evaluated by comparing the particle flux between the two scenarios and a variation of 10 to 20% is found, depending on R, with a mean value of 15%. The latter value is considered as the associated uncertainty.

The uncertainties in the hit rate from the FLUKA simulation and the GEANT4 detector simulation are added in quadrature. The total systematic uncertainty is about 14.5%.

7 Comparison of background modeling and experimental data

A comparison between simulation and measurement is used to validate the model presented in this study. Figure 10 compares the measured hit rate of Layer-2 of superchamber 28 with the prediction from simulation. The hit rate from simulation is obtained from the convolution of the average sensitivity shown in table 5 and the particle flux shown in figure 7 top-right. The data points in figure 10 correspond to different perpendicular distances R from the beamline to the centers of the η-sectors. As expected, the hit rate is higher at lower R (higher η) because the flux from the collision is higher in this region. The bottom panel of figure 10 shows the ratio of data to simulation and the estimated systematic uncertainty. The contributions from different types of particles to the total hit rate are shown in figure 11 for Layer-2. The largest contribution comes from neutrons while photons contribute about ∼15%. Charged hadrons and $e^\pm$ contribute about 1% only.
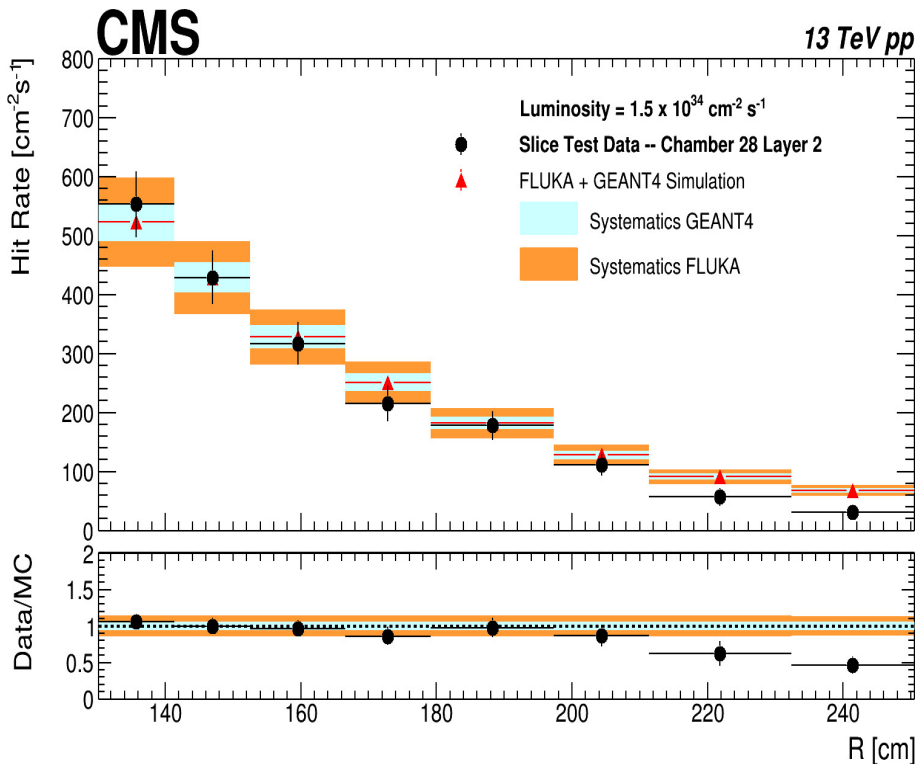

Figure 10. Comparison of the measured hit rates on Layer-2 of superchamber 28 in the slice test with the particle flux from the FLUKA simulation weighted by the sensitivity. The systematic uncertainties from the detector modelling (by the GEANT4 simulation) are shown as shaded blue bands around the prediction. The systematic uncertainties from the flux modelling for the CMS experimental configuration (by the FLUKA simulation) are shown as orange bands after adding them in quadrature with the systematic uncertainties shown in the blue band. The bottom panel shows the ratio of hit rates from data to those predicted from the simulation.
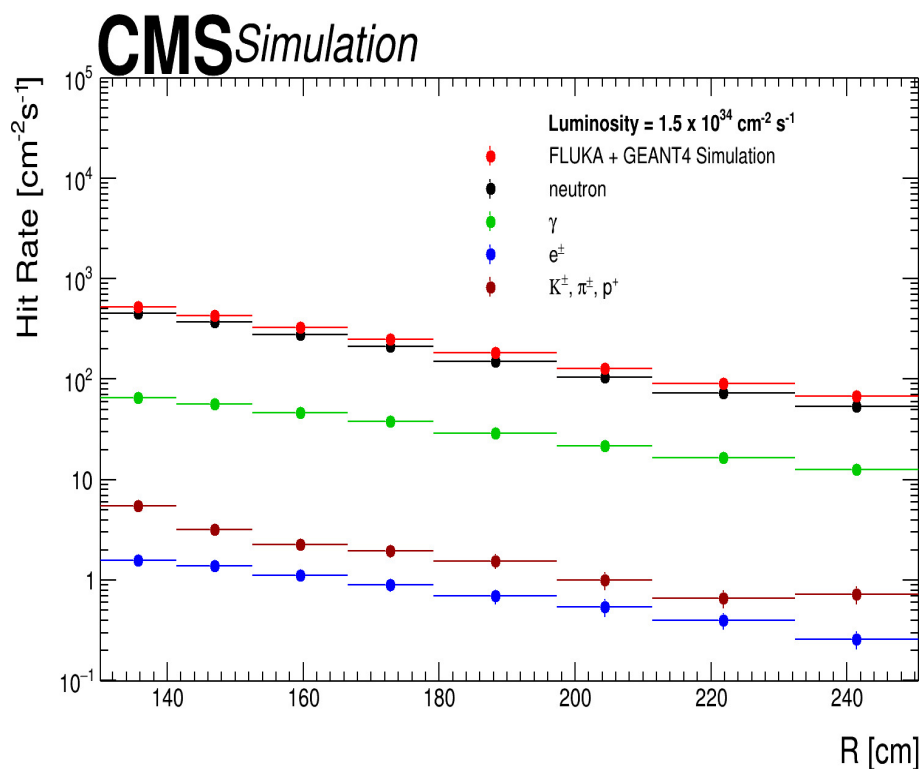
Figure 11. Prediction from simulation for hit rate contribution from different background particles at Layer-2 of superchamber 28.

The measured hit rates for the triple-GEM detector agree with those predicted from the simulation within the uncertainty except for η-sectors 1 and 2 for which data were taken with higher than nominal readout thresholds. The total uncertainty includes both the statistical uncertainty and the systematic uncertainties, described in the previous section, added in quadrature. The uncertainty of the hit rate in data includes the statistical uncertainty and uncertainties on the instantaneous luminosity measurement.

The hit rate data for i_η = 1 and 2 (sectors with R > 210 cm) in figure 10 are lower than the prediction. This can be explained by the higher than nominal thresholds for the VFAT-3 readout electronics during the data taking. The thresholds for i_η = 1 and 2 were 8.8 and 4.0 fC, respectively, corresponding to 6 and 3 electrons per strip in the drift gap. For i_η = 1, an energy loss of 168.6 eV (= 6 × 28.1 eV) is needed to count as a "hit", resulting in a low sensitivity. In this way, the applied thresholds caused a distortion of the strip multiplicity distributions for i_η = 1 and 2. The detection efficiency for muons at i_η = 1 was most affected by the higher threshold at the strip level. While a threshold of 3 fC is low enough for our simulation model to reasonably reproduce the data, a threshold of 8.8 fC is not low enough, especially since the interaction of particles with Ar/CO$_2$ gas (energy loss rate) [30] and electron multiplication (gas gain) are non-linear phenomena. While it is difficult to reproduce the non-linear effects in the current simulation framework a future study could be improved with a detailed description of the electron multiplication (avalanche) e.g. using the GARFIELD [31] software package, as well as a simulation of the electronics.

8 Summary

Collision-induced background hit rates in the CMS triple-GEM detector in pp collisions at the LHC were evaluated by modeling the radiation environment and detector response using a framework of the FLUKA and GEANT4 simulation packages. The FLUKA simulation provides kinetic energy and angular distributions of incident particles in the radiation environment. The GEANT4 simulation models particle interactions based on an accurate material description of each GEM detector. The simulated hit rates were obtained by combining the sensitivity and particle flux, and compared with measurements at a luminosity of 1.5×10^{34} cm^{-2} s^{-1} at 13 TeV. The predicted hit rates and experimental data are found to agree within their uncertainties for detector sectors with nominal operating parameters.

The framework presented in this article is generic, so it can be used for evaluation of hit rates on other detectors at High-Luminosity LHC, providing a better understanding of trigger rates and longevity of detectors.

Acknowledgments

References

[1] M. Huhtinen, *The radiation environment at the CMS experiment at the LHC*, master thesis, HU-SEFT-R-1996-14, Helsinki U. Tech., Helsinki, Finland (1996).

[2] Y. Musienko, A. Heering, R. Ruchti, M. Wayne, A. Karneyeu and V. Postoev, *Radiation damage studies of silicon photomultipliers for the CMS HCAL phase I upgrade*, *Nucl. Instrum. Meth. A* **787** (2015) 319.

[3] CMS collaboration, *The CMS muon project: technical design report*, Tech. Rep. CERN-LHCC-97-032, CERN, Geneva, Switzerland (1997) [CMS-TDR-3].

[4] R. Froeschl, M. Brugger and S. Roesler, *The CERN High Energy Accelerator Mixed Field (CHARM) facility in the CERN PS east experimental area*, in *Proceedings,* 12$^{\text{th}}$ *meeting of task-force on shielding aspects of accelerators, targets and irradiation facilities*, (SATIF-12), Batavia, IL, U.S.A., 28–30 April (2014).

[5] D. Pfeiffer et al., *The radiation field in the Gamma Irradiation Facility GIF++ at CERN*, *Nucl. Instrum. Meth. A* **866** (2017) 91 [arXiv:1611.00299].

[6] F. Sauli, *The Gas Electron Multiplier (GEM): operating principles and applications*, *Nucl. Instrum. Meth. A* **805** (2016) 2.

[7] CMS collaboration, *The CMS experiment at the CERN LHC*, 2008 *JINST* **3** S08004.

[8] A. Colaleo, A. Safonov, A. Sharma and M. Tytgat, *CMS technical design report for the muon endcap GEM upgrade*, Tech. Rep. CERN-LHCC-2015-012, CERN, Geneva, Switzerland (2015) [CMS-TDR-013].

[9] ALICE TPC collaboration, *Development of GEM-based read-out chambers for the upgrade of the ALICE TPC*, 2014 *JINST* **9** C04035.

[10] GEANT4 collaboration, *GEANT4 — a simulation toolkit*, *Nucl. Instrum. Meth. A* **506** (2003) 250.

[11] A. Ferrari, P.R. Sala, A. Fassò and J. Ranft, *FLUKA: a multi-particle transport code (program version 2005)*, CERN yellow reports monographs CERN-2005-010, CERN, Geneva, Switzerland (2005),

[12] CMS Muon Group collaboration, *Triple-GEM discharge probability studies at CHARM: simulations and experimental results*, 2020 *JINST* **15** P10013.

[13] D. Contardo, M. Klute, J. Mans, L. Silvestris and J. Butler, *Technical proposal for the phase-II upgrade of the CMS detector*, Tech. Rep. CERN-LHCC-2015-010, CERN, Geneva, Switzerland (2015) [LHCC-P-008] [CMS-TDR-15-02].

[14] CMS collaboration, *Background rate study for the CMS improved-RPC at HL-LHC using GEANT4*, *Nucl. Instrum. Meth. A* **936** (2019) 430.

[15] C.U. Estrada et al., *RPC radiation background simulations for the high luminosity phase in the CMS experiment*, 2019 *JINST* **14** C09045.

[16] F. Ivone, *Discharge mitigation strategies for the CMS GE1/1 triple-GEM detectors*, 2020 *JINST* **15** C05009.

[17] M. Abbas et al., *Detector control system for the GE1/1 slice test*, 2020 *JINST* **15** P05023.

[18] M. Abbas et al., *Performance of a triple-GEM demonstrator in pp collisions at the CMS detector*, 2021 *JINST* **16** P11014 [`arXiv:2107.09364`].

[19] GEANT4 collaboration, *Physics reference manual*, in *GEANT4 — a simulation toolkit. Manual* **1** (2019) 1.

[20] M. Abi Akl, O. Bouhali, A. Castaneda, Y. Maghrbi and T. Mohamed, *Uniformity studies in large area triple-GEM based detectors*, *Nucl. Instrum. Meth. A* **832** (2016) 1.

[21] A. Sharma, *Properties of some gas mixtures used in tracking detectors*, SLAC-J-ICFA-16-3, (1998) [SLAC-JOURNAL-ICFA-16-3].

[22] F. Sauli, *Principles of operation of multiwire proportional and drift chambers*, CERN-77-09, (1977).

[23] Geant4 collaboration, *Recent developments in GEANT4*, *Annals Nucl. Energy* **82** (2015) 19.

[24] D. Abbaneo, *Impact of the radiation background on the CMS muon high-eta upgrade for the LHC high luminosity scenario*, *PoS* **TIPP2014** (2014) 086.

[25] P. Aspell et al., *VFAT2: a front-end "system on chip" providing fast trigger information and digitized data storage for the charge sensitive readout of multi-channel silicon and gas particle detectors.*, *IEEE Nucl. Sci. Symp. Conf. Rec.* (2008) 1489.

[26] P. Aspell et al., *VFAT3: a trigger and tracking front-end ASIC for the binary readout of gaseous and silicon sensors*, *IEEE Nucl. Sci. Symp. Med. Imag. Conf. Rec.* (2018) 1.

[27] M. Abbas et al., *Performance of prototype GE1/1 chambers for the CMS muon spectrometer upgrade*, *Nucl. Instrum. Meth. A* **972** (2020) 164104.

[28] A. Howard, G. Folger, J.M. Quesada and V. Ivanchenko, *Validation of neutrons in GEANT4 using TARC data — production, interaction and transportation*, *IEEE Nucl. Sci. Symp. Conf. Rec.* (2008) 2885.

[29] J. Apostolakis et al., *Validation and verification of GEANT4 standard electromagnetic physics*, *J. Phys. Conf. Ser.* **219** (2010) 032044.

[30] Particle Data Group collaboration, *Review of particle physics*, *PTEP* **2020** (2020) 083C01.

[31] R. Veenhof, *GARFIELD, recent developments*, *Nucl. Instrum. Meth. A* **419** (1998) 726.